Self-Assembly and Integration of Ordered, Robust, Three-Dimensional Gold Nanocrystal/Metal Oxide Superlattices

Hongyou Fan[*,**], Kai Yang[***], John P. Gabaldon[**], Daniel M. Boye[*], Thomas Sigmon[***], Kevin J. Malloy[***], and C. Jeffrey Brinker[*,**]

[*]Sandia National Laboratories, Advanced Materials Laboratory, 1001 University Blvd. SE, Albuquerque, NM 87106. hfan@sandia.gov

[**]The University of New Mexico, Department of Chemical and Nuclear Engineering, Albuquerque, NM.

[***]The University of New Mexico, Center for High Technology Materials, Albuquerque, NM 87131.

ABSTRACT

We report the synthesis of a new nanocrystal (NC) mesophase through self-assembly of water-soluble NC-micelles with soluble silica. The mesophase comprises gold nanocrystals arranged within a silica matrix in a face-centered-cubic lattice with cell dimensions that are adjustable through control of the nanocrystal diameter and/or the alkane chain lengths of the primary alkanethiol stabilizing ligands or the surrounding secondary surfactants. Under kinetically controlled silica polymerization conditions, evaporation drives self-assembly of NC-micelles into ordered NC/silica thin film mesophases during spin-coating. The intermediate NC-micelles are water-soluble and of interest for bio-labeling. The robust, 3-D NC mesophase solids are of interest for development of collective optical and electronic phenomena, and, importantly, for the integration of nanocrystal arrays into device architectures. Initial experiments on a MOS capacitor fabricated with an ordered gold NC/silica 'oxide' demonstrated charge storage on the gold nanocrystals and discharge behavior dominated by electron transport within the ordered gold nanocrystal array.

Keywords: self-assembly, nanocrystals, superlattice, quantum dots, nanodevices

Nanometer-sized crystallites of metals, semiconductors, and oxides exhibit optical, electronic and chemical properties often different from those of the corresponding isolated molecules or macroscopic solids. The ability to adjust properties through control of size, shape, composition, crystallinity, and structure[1,2] has led to a wide range of potential applications for nanocrystals (NCs) in areas like optics, electronics, catalysis, magnetic storage, and biological labeling[3-6]. Furthermore NC assembly into 2- and 3-D arrays is of interest for development of synthetic solids with collective optical and electronic properties that can be further tuned by the nanocrystal spacing and arrangement[7,8]. For example, using uniformly-sized CdSe nanocrystals passivated with a close-packed monolayer of organic coordinating ligands (trioctylphosphine oxide), Murray *et al.*[9] exploited the inherent tendency for monodisperse lyophobic colloids to self-assemble to create periodic, three-dimensional quantum dot superlattices. Following this approach, Klimov *et al.*[10] prepared ordered CdSe quantum dot films and demonstrated optical gain and stimulated emission. In 2D quantum dot monolayers formed in a Langmuir trough, Collier *et al.*[11] reported quantum mechanical tunneling between adjacent silver nanocrystals at an interparticle spacing below 1.2-nm and a reversible insulator-to-metal transition below 0.5-nm. Even richer transport and collective phenomena are expected for 3-D NC arrays.

Despite recent advances in the synthesis and characterization of nanocrystals and nanocrystalline arrays, there remain numerous challenges that limit their practical utilization. For example, synthesis procedures generally used for metallic and semiconducting nanocrystals employ organic passivating ligands, making the nanocrystals water insoluble. This is very problematic for biological imaging and for incorporation of nanocrystals in hydrophilic sol-gel matrices like silica or titania needed for the fabrication of robust, functional lasers[12,13]. Furthermore, while steric stabilization of nanocrystals with organic passivating layers suppresses strong, attractive particle-particle interactions, thereby facilitating self-assembly of nanocrystal arrays, it necessarily causes the arrays to be mechanically weak and often thermally and chemically unstable. This ultimately limits routine integration of NCs into devices.

Here we describe the direct synthesis of water-soluble nanocrystalline gold micelles (NC-micelles) and their further self-assembly with silica into robust, ordered 3-dimensional nanocrystalline arrays in bulk or thin film forms. The synthetic approach is general and avoids the complicated multi-step procedures reported previously[14]. Our concept is to consider monosized, organically-passivated nanocrystals as large hydrophobic molecules that, if incorporated individually into the hydrophobic interiors of surfactant micelles, would result in the formation of monosized NC micelles composed of a metallic (or other) NC core and a hybrid bilayer shell with precisely defined primary and secondary layer thicknesses (see Fig. 1H). The hydrophilic NC micelle surfaces would cause them to be water-soluble and allow further assembly or derivatization as depicted in Fig. 1.

To individually incorporate NCs in surfactant micelles and realize this concept, we developed a micro-emulsion procedure[15]. A concentrated nanocrystal solution, prepared in organic solvent (chloroform, hexane,

etc.), is added to an aqueous solution of surfactant with a volume ratio of 1:10 under vigorous stirring to create an

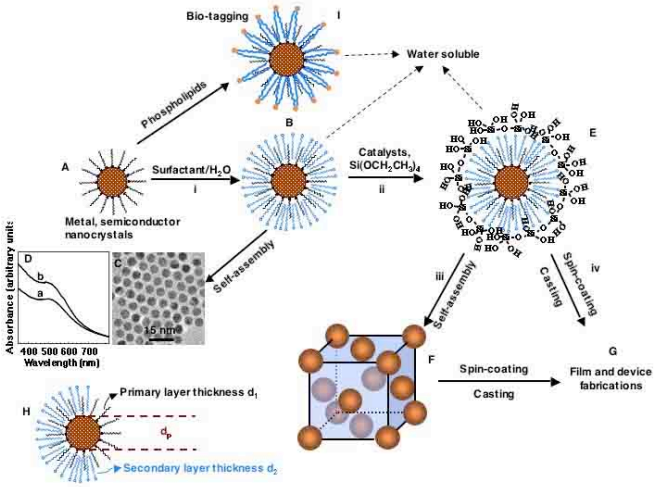

Figure 1. Processing diagram for the synthesis of water-soluble gold nanocrystal micelles and periodically ordered gold NC/silica mesophases. (A) Gold nanocrystals were prepared according to the method of Brust *et al.*[21], using 1-dodecanethiol (DT) as a stabilizing agent. (B) Thiol-stabilized nanocrystals are encapsulated in surfactants to form water-soluble NC micelles that, upon evaporation, self-assemble to form hexagonally-ordered NC arrays as shown in the TEM image (C). (D) UV-visible spectra of (a) gold nanocrystals in chloroform and (b) gold NC-micelles in water both exhibit plasmon resonance bands at 510-cm^{-1}. (E) Silicic acid moieties formed by hydrolysis of TEOS are organized at the hydrophilic surfactant-water interface of NC micelles, leading, under basic conditions, to a gold NC/silica mesophase (F) composed of NCs organized in a periodic FCC lattice within a dense silica matrix. (G) Under acidic conditions that suppress siloxane condensation, spin-coating or casting result in ordered thin film NC/silica mesophases that are readily integrated into devices. (H) The lattice constant of the NC/silica mesophase is controlled by the nanocrystal size (d_p), the primary layer thickness of the alkanethiol, d_1, and/or the secondary layer thickness of the surfactant, d_2 (see Fig. 3). I. Polyethylene glycol-surfactants or lipids can be used to prepare biocompatible water-soluble NC micelles for biolabeling[6].

oil-in-water micro-emulsion. Organic solvent evaporation (aided optionally by vacuum or heat treatments) transfers the NCs into the aqueous phase by an interfacial process driven by the hydrophobic van der Waals interactions between the primary alkane of the stabilizing ligand and the secondary alkane of the surfactant, resulting in thermodynamically defined interdigitated bilayer structures (Fig 1H). For single-tailed surfactants, an alkane chain of eight or more carbons is required to form micelles with gold nanocrystals stabilized by C_{12} alkanethiols (dodecanethiol). Cationic, anionic, and non-ionic surfactants can all form NC-micelles, allowing facile control of micelle surface charge and functionality. In addition, fluorescent semiconducting CdSe NCs (stabilized by trioctylphosphine oxide) have been formed into NC-micelles with maintenance of optical properties, further supporting the general nature and flexibility of this approach.

NC-micelle solutions are colored and indefinitely stable (> 2-years). The formation of individual gold NC-micelles was confirmed by UV/visible spectroscopy (Fig. 1D), where we observe no difference in the position or

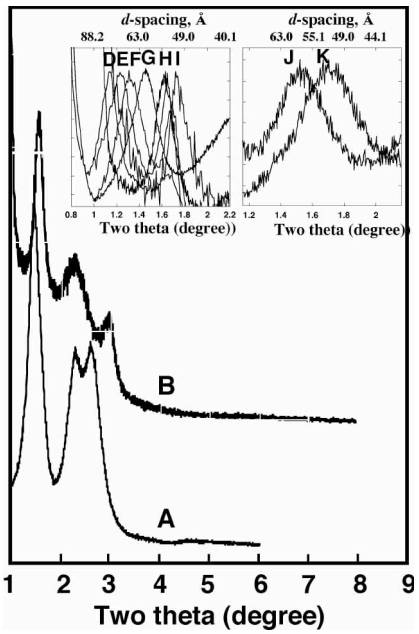

Figure 2. Representative x-ray diffraction (XRD) patterns of gold NC/silica mesophases. (A) XRD patterns of bulk gold NC/silica samples prepared according to pathway i-ii-iii (Fig. 1) by addition of NaOH to an aqueous solution containing TEOS and gold NC-micelles. (B) Gold NC/silica thin film mesophase formed by spin-coating (Fig. 1, pathway i-ii-iv). The pattern can be indexed as an FCC cubic mesostructure with lattice constant a = 95.5Å. Insets: traces (F) through (K) are magnifications of the (111) reflections plotted linearly for samples prepared as in (B) using gold nanocrystals with successively smaller diameters (F~33Å, G~27Å, H~23Å, I~17Å, J~12Å, K~11Å). Traces (L) and (M) are magnifications of the (111) reflections plotted linearly for samples prepared as in (B) with two different secondary alkane chain lengths of the surfactant $(CH_3(CH_2)_n(NCH_3)_3^+Br^-$, n_L=15, n_M=11).

width of the plasmon resonance band (~510-nm) of the C_{12}-alkanethiol stabilized gold NCs in chloroform and the resulting water soluble NC-micelles. In addition, evaporation of the NC-micelles resulted in self-assembly of hexagonally ordered NC arrays (Fig.1C) as expected for individual, monosized nanocrystals[16].

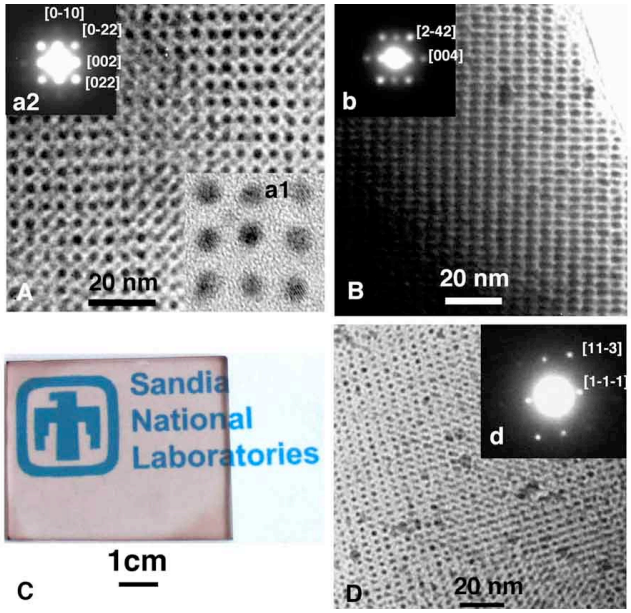

Figure 3. Representative transmission electron microscope (TEM) images of gold nanocrystal/silica mesophases. (A) and (B) [100] and [210] orientations of bulk samples prepared according to pathway i-ii-iii (Fig 1) and corresponding to Fig. 2, trace B. Inset (a1): high resolution TEM of sample (A) showing gold NC lattice fringes. Inset (a2): selected area diffraction pattern from the image in (A). Inset (b) selected area electron diffraction from the image in (B). (C) Optical image of ordered gold NC/silica thin film spin-coated on glass. (D) TEM image of [211]-oriented NC/silica thin film mesophase. Inset (d) selected area diffraction pattern from image in (D).

Addition of tetraethyl orthosilicate under basic conditions results in the formation of hydrophilic oligo-silicic acid species that organize with NC-micelles to form a new type of ordered gold NC/silica mesophase with face-centered-cubic symmetry (space group Fm3m). Figure 2B shows a representative low angle x-ray diffraction pattern of a nanocrystal mesophase powder prepared according to pathway i-ii-iii (Fig.1) using 2-nm diameter C_{12}-thiol stabilized gold NCs, cetyltrimethylammonium bromide (C_{16}TAB) surfactants, and sodium hydroxide catalyst. Based on FCC symmetry the primary peaks are assigned as 111, 220, and 311 reflections. Figures 3A and B show representative TEM images of [001]- and [012]-oriented nanocrystal mesophases (prepared as for Fig. 2B) along with their corresponding electron diffraction patterns. The TEM images are consistent with an FCC unit cell with a = ~10.2 nm and a uniform, minimum (silica/surfactant) spacing between NCs of ~6 nm. This appears to be the first example of an ordered FCC nanocrystal array formed spontaneously by self-assembly in aqueous media (rather than by solvent evaporation[5,9,16]. Compared to other ordered NC arrays, the embedding silica matrix provides for greater chemical, mechanical, and thermal robustness and, compared to other connected NC systems (for example, those prepared by DNA hybridization[18,19], thermodynamically controlled self-assembly provides greater order and control of NC spacing.

Insets F through K in Fig. 2 show the (111) d-spacing to change linearly from *ca* 5.0 to 7.2-nm through variation of d_p from 1.0 to 3.3-nm. Insets L and M show that changing the secondary layer thickness d_2 by 4 carbon units ($CH_3(CH_2)_n(NCH_3)_3^+Br^-$, n_L=11 to n_K=15) results in a 1.11-nm change in (111) d- spacing (1.38-Å/C-C bond) consistent with model predictions and structural studies.

Using acidic conditions designed to minimize the siloxane condensation rate (pH~2), pathway i-ii-iv (Fig. 1) leads to the formation of thin films using standard techniques like dip-coating, spin-coating, or micro-molding. By suppressing siloxane condensation and, thereby, gel formation, solvent evaporation accompanying coating induces self-assembly of NC-micelles into FCC nanocrystal thin film mesophases (Fig. 3D) in a manner similar to the evaporation-induced self-assembly of cubic or hexagonal silica/surfactant thin film mesophases[20,22]. The thin film XRD pattern (Fig. 2A) is consistent with a slightly distorted FCC mesophase (face-centered tetragonal) due to constrained one-dimensional shrinkage normal to the substrate surface, observed consistently for thin film mesophases as a result of siloxane condensation[23]. TEM images of films (e.g. Fig. 3D) are qualitatively similar to those of powders, although both XRD and TEM indicate a slightly reduced unit cell dimension (a = ~9.6 nm).

As an initial investigation of charge transport in our ordered three-dimensional nanocrystal arrays, we fabricated planar metal-oxide-semiconductor (MOS) devices (see schematic in Fig. 4) with a gold NC/silica mesophase 'oxide' prepared according to pathway i-ii-iv (Fig. 1) and structurally equivalent to thin film samples in Figs. 2A and 3D. Charge storage and decay was assessed by measuring the time and voltage behavior of the capacitance.

Figure 4 presents the results of electric field-aided transport measurements performed on both types of MOS devices. For this measurement the sample is initially biased at V_1 for 50 seconds, then rapidly switched (<1μs) to V_2 and the time evolution of the capacitor charge monitored. Samples without gold exhibit an exponential discharge (with a time constant ~100 μs) consistent with normal RC discharge behavior. For the samples with gold, an ogive (S-shaped) profile with a ~7.5 second discharge time is observed. The total excess charge contained in this capacitor is approximately 2.8 x 10^{-11} C. Assuming the capacity of each nanocrystal to be one electron based on electrostatic energy considerations, this corresponds to 10^{18} cm^{-3} charged NCs. We attribute this to the charging of the gold in the oxide near the gate electrode when the gate is negatively biased. A diagram depicting the charges within the oxide and p-doped Si substrate is shown in Fig. 4C for the gate bias sequence studied. After reversing the gate voltage to V_2, the electrons on the gold NCs are swept out of the oxide into the gate sequentially from the gate side first. No change in substrate capacitance occurs until the

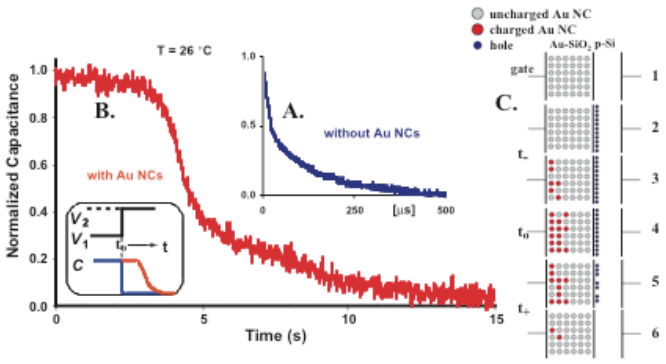

Figure 4. Time dependence of normalized capacitance for MOS capacitors prepared using silica or ordered gold NC/silica (Fig. 3D) as the 'oxide' dielectrics. The charge is measured when the capacitors are switched from V_1 to V_2. The discharge time for capacitors without gold NCs (A) is exponential with a characteristic time constant of ~100 μs. For gold NC-containing capacitors (B), the decay is no longer exponential and the discharge time (10 to 90%) is about 7.5 seconds. The time behavior of the discharge curve may be explained by following the biasing sequence in (C). Diagram 1 depicts an unbiased neutral p-type Si substrate. 2) shows that once a negative bias V_1 is placed on the gate, an accumulation of holes is quickly established at the Si-oxide interface. In 3) the capacitance of the device with gold NCs is higher than that of an equivalent gold NC-free device due to the excess stored charge in the gold levels. Experiments indicate that this process continues until all of the gold NC's in the first 25% of the oxide film near the gate are charged. Upon reduction of the gate bias to V_2 in 4), the accumulation layer begins to disappear. However, in 5) the accumulation layer is partially sustained in the presence of the charged gold NCs. Only as the electrons on the gold NCs move into the gate does the accumulation layer dissipate completely as shown in 6). The minimum capacitance for these structures occurs when the p-type semiconductor surface is biased into inversion. This value is the same for both gold NC and NC-free capacitors.

gold NCs in the oxide are discharged as they effectively pin the Si-surface in accumulation. Using the FCC lattice constant, we estimate a uniform gold NC concentration in the oxide of ~$4x10^{18}$ cm^{-3}. However, only those NCs located near the gate electrode can respond to the high frequency signal used to measure the capacitance, resulting in roughly *all* of the NCs in the first 25% of the oxide film being occupied by electrons. Given the spacing for these dots, we expect coulomb blockade effects to control transport amongst the gold NCs. However, disorder and trapping within the silica matrix could prevent collective effects, so transport in this situation is probably also influenced by a combination of local kinetic and diffusive factors, particularly at room temperature where these experiments were performed. Still, in that we observe charge storage and transport behavior that is completely different from that of the corresponding MOS capacitor prepared *sans* gold with silica identical to the host matrix of the NC array, it is evident that charge is stored on the gold NCs and that the discharge characteristics are dominated by electron transport involving the nanocrystals.

ACKNOWLEDGEMENT

This work was partially supported by the U.S. Departmentof Energy (DOE) Basic Energy Sciences Program, Sandia National Laboratory's Laboratory Directed R&D program, Center for Integrated Nanotechnology, the Air Force Office of Scientific Research, and DARPA. TEM investigations were performed in the Department of Earth and Planetary Sciences at the University of New Mexico. Sandia is a multiprogram laboratory operated by Sandia Corporation, a Lockheed Martin Company, for DOE under contract DE-AC04-94ALB5000.

REFERENCES

[1] M. A. El-Sayed, *Accounts of Chemical Research* **34**, 257-264 (2001).
[2] Y. G. Sun, Y. N. Xia, *Science* **298**, 2176-2179 (2002).
[3] C. B. Murray, *et al*., *Annu. Rev. Mater. Sci.* **v.30** 545-610, 2000).
[4] A. P. Alivisatos, *Science* **271**, 933-937 (1996).
[5] S. H. Sun, *et al*., *Science* **287**, 1989-1992 (2000).
[6] B. Dubertret *et al.*, *Science* **v.298**, p.1759-1762 (2002).
[7] R. Elghanian, *et al*., *Science* **277**, 1078-1081 (1997).
[8] R. P. Andres, et al., *Science* **273**, 1690-1693 (1996).
[9] C. B. Murray, C. R. Kagan, M. G. Bawendi, *Science* **270**, 1335-1338 (1995).
[10] V. I. Klimov *et al.*, *Science* **290**, 314-317 (2000).
[11] C. P. Collier, *et al*., *Science* **277**, 1978-1981 (1997).
[12] V. C. Sundar, *et al*., *Advanced Materials* **14**, 739 (2002).
[13] M. A. Petruska, *et al,*, *Adv. Mater.* **15**, 610-613 (2003).
[14] M. Bruchez, *et al, Science* **281**, 2013-2016 (1998).
[15] H. Fan, et al., *Science* **304**, 567-571 (2004).
[16] Z. L. Wang, *Adv. Mater.* **v.10**, p.13-& (1998).
[17] J. Beck *et al.*, *J Am Chem Soc* **114**, 10834-10834 (1992).
[18] A. P. Alivisatos *et al.*, *Nature* **v.382**, p.609-611 (AUG 15 1996, 1996).
[19] C. A. Mirkin, *et al.*, *Nature* **v.382**, p.607-609 (1996).
[20] Nitrogen sorption isotherms of ordered gold nanocrystal/silica measured by surface acoustic wave (SAW) technique show no nitrogen sorption.
[21] M. Brust, *et al*., *Chemical Communications*, 801-802 (1994).
[22] Y. Lu *et al.*, *Nature* **389**, 364-368 (1997).
[23] D. A. Doshi *et al.*, *Science* **290**, 107-111 (2000).